Journal of The Electrochemical Society, **154** (9) D443-D451 (2007)
0013-4651/2007/154(9)/D443/9/$20.00 © The Electrochemical Society

Electrodeposition of Ni in Submicrometer Trenches

S.-K. Kim,[a] J. E. Bonevich, D. Josell, and T. P. Moffat[*,z]

Materials Science and Engineering Laboratory, National Institute of Standards and Technology, Gaithersburg, Maryland 20899, USA

A survey of the effect of cationic, anionic, and nonionic surfactants on the rate and morphological evolution of nickel electrodeposition is presented. Attention is given to the prospect for void-free filling of submicrometer trenches. Cationic species such as polyethyleneimine (PEI) and cetyl-trimethyl-ammonium (CTA +) yield significant inhibition of nickel deposition. For a range of concentrations the single cationic surfactant systems exhibit hysteretic voltammetric curves that, when corrected for ohmic electrolyte losses, reveal an S-shaped negative differential resistance. Void-free bottom-up superconformal feature filling is observed when operating at potentials within the hysteretic regime whereby metal deposition begins preferentially in the most densely patterned regions of the wafer followed by propagation of the growth front laterally across the wafer surface. In contrast, at low overpotentials and concentrations, sulfur-bearing additives such as thiourea (TU) exert a depolarizing effect on nickel deposition and negligible hysteresis. When PEI and TU are both present, the suppression provided by PEI is diminished and feature filling leads to uniform deposition on the wafer scale. Suitable combinations of PEI and TU enable near void-free filling of ≥230 nm wide trenches with sloping (∼3.5°) sidewalls. Initial conformal growth is followed by geometric leveling once the deposits on the sloping sidewalls meet.

Manuscript submitted March 13, 2007; revised manuscript received April 25, 2007. Available electronically July 2, 2007.

One of the challenges in manufacturing three-dimensional (3D) structures associated with ultralarge-scale integration (ULSI), microelectromechanical systems (MEMS), and 3D packaging is achieving void-free filling of trenches and vias. Two different processing schemes known as through-mask plating (or LIGA)[1] and Damascene processing,[2] respectively, have emerged. In through-mask plating, metal deposition occurs on the exposed areas of an otherwise-blocked electrode. Two manifestations of this are metal plating in nanopores of a metal-backed anodized alumina membrane[3] and selective plating on a metallized substrate patterned with an overlying insulating photoresist.[2] In contrast, the demands of producing multilevel wiring for microelectronic interconnects has spawned the Damascene process whereby a 3D patterned surface is first metallized to ensure conductivity across the entire surface,[2] and void-free bottom-up superconformal filling of the trenches and vias is then accomplished through the effect of competitive adsorption of accelerating and inhibiting electrolyte additives combined with the consequences of area change.[4] The resulting superconformal deposition mode, called "superfilling," has been quantitatively described in terms of a curvature enhanced adsorbate coverage model. Through-mask deposition has been applied to a wide variety of materials ranging from metals to semiconductors, including applications in both passive and active devices. In contrast, the Damascene electrodeposition filling process has been limited to passive metal conductors such as copper,[4] silver[5,6] and gold.[7,8] At this juncture it is interesting to see if the bottom-up superfilling process can be extended to ferromagnetic materials that might be useful as active device elements in ULSI and MEMS. A variety of device geometries can be imagined from partially filled trenches, i.e., horseshoe magnets, or vias, i.e., magnetic cylinders, to completely filled trench or via structures that are embedded in a magnetically isolated, nonferrous environment, etc. In this paper, nickel deposition was examined as a prototypical case of magnetic material with full recognition that the results are likely to also be applicable to the deposition of cobalt, iron, and alloys thereof.[9,10]

A survey of the effect of various electrolyte additives on the nickel deposition kinetics, as revealed by voltammetric and chronoamperometric measurements, is presented. This is complemented by studies of feature filling that reveal a range of interesting effects on morphological evolution. Filling studies were performed at modest potentials and current density where negligible depletion of the nickel cations occurs, simplifying the analyses. Likewise, the studies were performed at pH 3, which minimized the parasitic effects of hydrogen evolution on the voltammetric measurements and avoided potential complications associated with the H_2 bubbles that form readily in more acidic electrolytes. As a point of departure the effects of prototypical cationic, anionic, and nonionic surfactants on the nickel deposition were examined. The survey is far from exhaustive, and the molecules examined were largely selected from prior reports of conventional Ni leveling[11-23] as well as Cu electroplating and superfilling.[23-30]

Experimental

Ni electrodeposition was studied using a variant of a Watts bath composed of 1 mol/L $NiSO_4 \cdot 6H_2O$, 0.2 mol/L $NiCl_2 \cdot 6H_2O$, and 0.5 mol/L H_3BO_3 dissolved in 18 MΩ cm deionized water. The working electrode for the electrochemical analysis was an oxygen-free, high-conductivity Cu plate sequentially polished from 350 to 2400 grade SiC papers. The working electrode was covered with 3M plater's tape that had been punched to define a circular working area of 2.62 cm^2. A nickel plate and a saturated calomel electrode (SCE) were used as the counter and reference electrodes, respectively. The cell for the electrochemical experiments was a Teflon cylinder of 5 cm diameter and 8.5 cm height with parallel, vertically oriented working and counter electrodes separated by a distance of 1.3 cm. The SCE reference electrode was placed midway between the working and counter electrode but laterally positioned so as not to interfere with the current distribution between the other electrodes. A distance of 1.8 cm separated the working and reference electrode and impedance measurements revealed an uncompensated ohmic resistance of 9.35 Ω cm^2.

The effect of a variety of organic additives on the nickel deposition rate was assessed using slow sweep rate (1 mV/s) voltammetry. The species examined were drawn from previous reports of additive-induced inhibition and/or acceleration in nickel[9-23] and copper[23-30] plating systems. Potential suppressor or rate-inhibiting species include dodecyltrimethylammonium chloride [DTAC, $CH_3(CH_2)_{11}N^+(CH_3)_3Cl^-$; Fluka[b]], dodecyltrimethylammonium bromide [DTAB, $CH_3(CH_2)_{11}N^+(CH_3)_3Br^-$]; sodium dodecyl sulfate [SDS, $CH_3(CH_2)_{11}OSO_3^-Na^+$; Fisher], 2-butyne-1,4-diol (2-B-1,4-D, $HOCH_2C{\equiv}CCH_2OH$, Aldrich), saccharin ($C_7H_5NO_3S$, Aldrich), sodium benzenesulfonate (SBS, $C_6H_5SO_3^-Na^+$, Aldrich), cetyltrimethylammonium chloride

---

[*] Electrochemical Society Active Member.
[a] Present address: Center for Fuel Cell Research, Korea Institute of Science and Technology, Cheongryang, Seoul 130-650, Korea.
[z] E-mail: thomas.moffat@nist.gov

[b] The names of companies and products are included for completeness of description. They do not imply NIST endorsement.

[CTAC, $CH_3(CH_2)_{15}N^+(CH_3)_3Cl^-$; Alfa Aesar], polyethyleneimine {PEI,-[$NH_2^+CH_2CH_2NH^+(CH_2CH_2NH_3^+)CH_2CH_2^-$]$_n$, 1800 Mw; branched, Alfa Aesar}, 4-picoline ($CH_3C_5H_4N$, Alfa Aesar), polyethylene glycol [PEG, (-CH_2CH_2O-)n, 3400 Mw; Aldrich]. Some sulfur-containing organic additives, such as thiourea (TU, H_2NCSNH_2, Alfa Aesar), 3-mercapto-1-propane sulfonic acid, sodium salt [MPS, $HS(CH_2)_3SO_3^-Na^+$, Raschig], bis(3-sulfopropyl) disulfide, sodium salt [SPS, $Na_2^+[SO_3^-(CH_2)_3S]_2$, Raschig], and 3-*N*,*N*-dimethylaminodithiocarbamoyl-1-propane sulfonic acid, sodium salt [DPS, $Na^+SO_3^-(CH_2)_3SCSN(CH_3)_2$, Raschig] were investigated as potential accelerating or depolarizing additives. For the survey, the concentrations of the suppressors were fixed at 100 μmol/L with the exception of PEI that exhibited similar inhibition at much lower concentrations.[28] In order to more fully characterize the effect of PEI the concentration was varied from 2 to 200 μmol/L. For comparison to the rate-suppressing additives, accelerating sulfur-bearing species were surveyed using a fixed concentration of 100 μmol/L. This concentration is within the reported depolarizing regime for TU, a bifunctional additive that exhibits an accelerating effect at low concentrations and an inhibiting effect at higher concentrations.[11,12,20] Similar behavior has been reported for DPS on Cu deposition.[27]

Feature filling was examined using Cu-seeded trenches approximately 770 nm deep and 5 μm to 210 nm wide to probe the effect of the suppressing and accelerating additives as well as combinations thereof. Depositions were conducted at −0.9 V vs SCE for 3 min in the base electrolyte with designated concentrations of the additives. In order to minimize seed-layer corrosion the specimens were immersed into the electrolyte with the potential applied. Feature filling was also examined as a function of deposition time. Specimen cross sections obtained by mechanical polishing followed by ion milling were examined by field emission scanning electron microscopy (FESEM). A subset of samples was also prepared by a single-step focus ion beam milling and examined by SEM. Filled features were also examined by transmission electron microscopy of cross sections prepared using traditional dimpling and ion-milling methods.

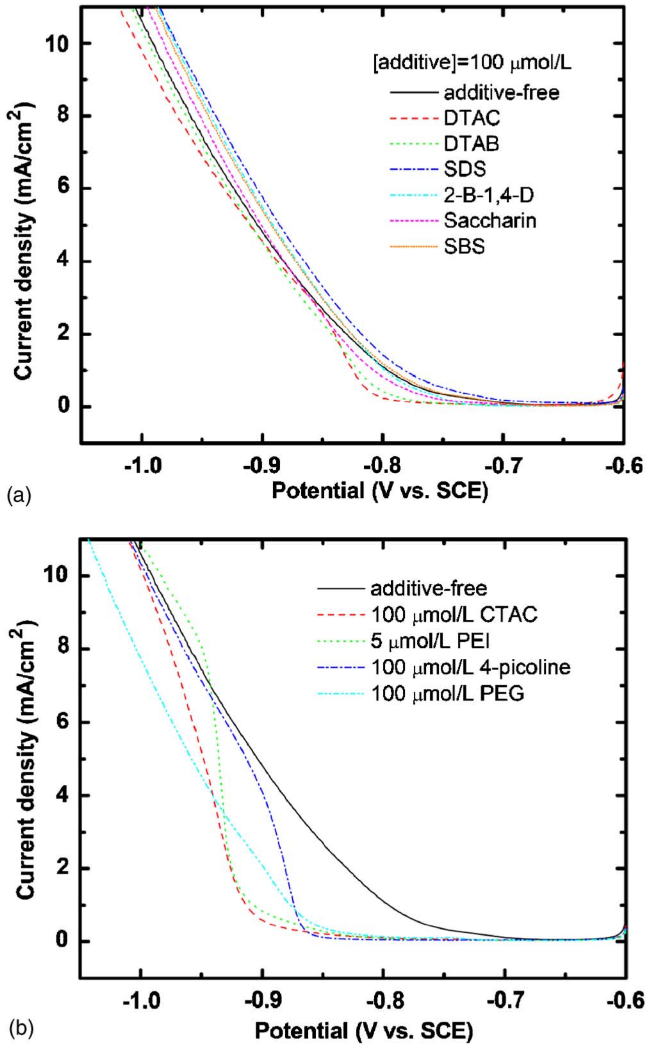

Figure 1. (Color online) Slow sweep voltammetry survey of the effect of cationic, anionic, and nonionic surfactants on Ni deposition from an electrolyte of 1 mol/L $NiSO_4 \cdot 6H_2O$ + 0.2 mol/L $NiCl_2 \cdot 6H_2O$ + 0.5 mol/L H_3BO_3. The sweep rate was 1 mV/s. (a) Results for additives having no, or minimal, polarizing effect. (b) Results for additives that significantly inhibit the nickel deposition.

Results and Discussion

Inhibitors.— A voltammetric survey of the influence of rate suppressing additives on the kinetics of Ni deposition is presented in Fig. 1. The results were separated into two groups on the basis of the observed inhibition: ineffective (Fig. 1a) and effective (Fig. 1b). The voltammetric curve for the additive-free Ni electrodeposition shows an onset of deposition between −0.65 and −0.70 V followed by a linear characteristic at higher overpotentials, i.e., where the current density is greater than 20 mA/cm^2, (not shown) that reflects the considerable electrolyte resistance associated with the system. Evaluation of the reciprocal of the slope for the additive-free system between 60 mA/cm^2 at −1.45 V and 20 mA/cm^2 at −1.1 V yields an electrode area normalized solution resistance of 8.75 Ω cm^2 that is consistent with the value of 9.35 Ω cm^2 determined by high-frequency impedance measurements. The additives examined in Fig. 1a include a negatively charged C_{12} surfactant (SDS), a diol with an unsaturated hydrocarbon chain (2-B-1,4-D), a negatively charged aromatic compound (SBS), and heterocyclic aromatic compound (saccharin), all of which have previously been studied for Ni electrodeposition.[11-23] At first glance, none of these additives exert a significant effect on the voltammetric behavior of Ni deposition for the concentration examined. In contrast, the cationic surfactants DTAB, DTAC, 4-picoline, CTAC, and PEI all exhibit some degree of inhibition, as shown Fig. 1a and b. The voltammetric curves have a hysteretic character whereby the inhibition evident at small overpotentials is followed by abrupt breakdown and reversion to the response of the additive-free system for the remainder of the voltammetric sweep (including the return scan). The position of the breakdown or critical potential is a function of the surfactant species: −0.87 V for 4-picoline and ∼−0.92 V for CTAC and PEI, as shown in Fig. 1b, while weaker inhibition is provided by DTAC and DTAB with the critical potential being near −0.81 V, as shown in Fig. 1a.

Based on the literature correlations[31] between the point of zero charge (pzc) and work function values, it is anticipated that the Ni surface is negatively charged under the given deposition conditions. Thus, one plausible origin of the inhibition of the nickel deposition reaction may be an ion-pairing interaction between the surface and the cationic surfactant that blocks access of nickel cations to the electrode. The observation that CTAC is more effective compared to DTAC or DTAB indicates that some contribution related to hydrophobicity (C_{16} vs C_{12}) is also important. As the pyridine derivative 4-picoline has suppressor characteristics that lie between that of DTAC, DTAB, and PEI/CTAC, it would appear that the strength of the hydrophobic interaction associated with the aromatic rings lies between that provided by the C_{16} vs C_{12} alkane chains. As shown in Fig. 1b, PEI is a particularly effective suppressor. The nitrogen-bearing weak polyelectrolyte has a pK_a (pH) of ∼10.4,[32] such that the numerous (∼40) imine groups within a given molecule can acquire a positive charge via protonation in the acidic Watts bath.

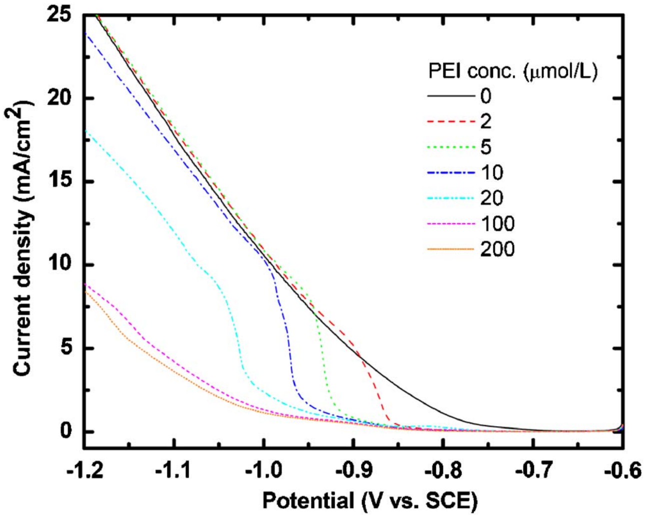

Figure 2. (Color online) PEI concentration strongly influences the slow sweep voltammetry of Ni deposition from 1 mol/L $NiSO_4 \cdot 6H_2O$ + 0.2 mol/L $NiCl_2 \cdot 6H_2O$ + 0.5 mol/L H_3BO_3. The sweep rate was 1 mV/s. Inhibition increases monotonically as PEI concentration is increased from 0 to 200 μmol/L. Inhibition breaks down at increasingly more negative potentials as PEI concentrations increases to 5 μmol/L and subsequently, the additive-free deposition kinetics prevail.

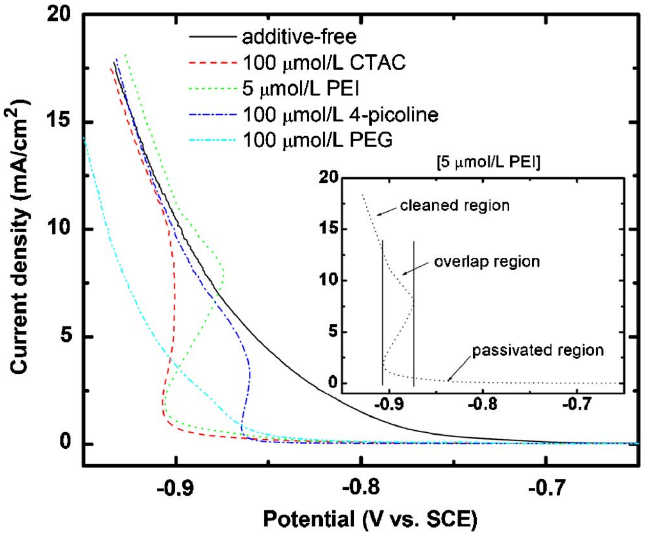

Figure 3. (Color online) S-NDR is revealed in the voltammograms of Fig. 1b once they are corrected for the IR voltage drop associated with the resistive electrolyte. The multiplicity of current values for a given potential gives rise to strong nonlinear active-passive behavior. The three different regimes of behavior are indicated in the insert.

The multiple cationic sites per molecule also account for the low (5 μmol/L) PEI concentration required to achieve substantial inhibition.

The nonionic polymer PEG also exerts strong inhibition that is sustained over the entire potential range shown in Fig. 1b. Negligible hysteretic character is evident and an identical response is observed for a lower, e.g., 50 μmol/L, PEG concentration (not shown). This is similar to the saturated suppression behavior observed for a PEG-Cl blocking layer in the copper system and can be described in terms of a simple area blockage model that includes a persistent "leakage current" resulting in spatially uniform deposition across the work piece.[26,33]

In contrast to PEG, inhibition derived from PEI exhibits a strong dependence on concentration. As shown in Fig. 2, the critical potential shifts systematically to more negative potentials with increasing PEI concentration. For concentrations up to 10 μmol/L PEI, the kinetic response reverts to additive-free behavior beyond the critical potential; this gives rise to a well-defined hysteretic response. For concentrations beyond 10 μmol/L, inhibition continues to increase; however, the hysteretic response is attenuated and the additive-free kinetic response is no longer observed. By 20 μmol/L, PEI suppresses deposition as effectively as PEG over the full potential range, although the rough character of the curve suggests unstable behavior. For PEI concentrations of 100 μmol/L and above, the inhibition saturates and negligible hysteresis is seen.

The abrupt breakdown of inhibition characterized by the critical potential most clearly evident for PEI, CTAC, and 4-picoline deserves further analysis. When the experimental voltammetric results are corrected for the uncompensated solution resistance, a negative differential resistance (NDR) in the interface kinetics is revealed as shown in Fig. 3. (This postexperiment correction does not consider the nonlinear distortions of the actual sweep rate associated with the ohmic drop, the magnitude of which scales with current density.) The S-shaped NDR (S-NDR) region corresponds to the existence of two stable states for a given potential. Such bifurcation processes have a rich history in electrochemistry, ranging from studies of active-passive transitions of corroding metals to electrocatalytic processes, all of which have been connected with pattern formation via the coupling of interface kinetics and transport processes.[34] For the case of additive plating, a steady-state model is available that couples mass-transport-limited adsorption of a blocking additive and current-density-dependent removal of the blocking additive from the surface by incorporation into the growing deposit, the latter representing a positive feedback term.[35] In the absence of significant ohmic losses in the electrolyte such bistable NDR systems move rapidly between the two states depending on the experimental conditions.[34,35] In the presence of significant ohmic losses in the electrolyte the NDR is obscured and the voltammetric response exhibits only a monotonic slope, as evident in Fig. 1b and 2. Importantly, in related activated-inhibitor coupled systems, the combination of NDR with a distributed electrical potential has been shown to give rise to standing Turing-type patterns on the electrode.[34,36] In the present case the patterned substrate provides a perturbation on the mass-transport conditions as a function of position while the finite seed-layer resistance combines with the electrolyte resistance to perturb the electrical distribution during metal deposition. Preliminary feature-filling experiments, as detailed in a later section, provide some evidence for such patterning effects in this system.

Accelerators.— Voltammetry was also used to identify depolarizing additives for Ni electrodeposition; the results are summarized in Fig. 4. Four sulfur-containing additives were examined: TU, SPS, MPS, and DPS. TU, one of the most investigated additives in Ni electrodeposition, can either accelerate or inhibit the deposition reaction depending on its concentration in the electrolyte. The shift from depolarizing to polarizing influence has been reported to occur at concentrations between several hundreds μmol/L and several mmol/L.[11,12,20] Successful leveling during Ni electrodeposition using the suppression effects associated with higher concentrations of TU has been reported.[11,19] There is also one report of TU-derivatized electrodes becoming bright during nickel plating in the absence of TU.[37] This report, along with similar observations reported in the case of copper plating, motivated the investigation detailed herein.[4,24,25,38,39] The depolarization associated with low TU concentrations in the electrolyte has been ascribed to the sulfide generated during electrochemical reduction of sulfur associated with the decomposition of TU at the cathode surface during the Ni deposition.[20] The characteristic reduction potential for such TU decomposition to sulfide ion has been attributed to a voltammetric wave near −0.7 V vs SCE.[17] A similar reduction wave is evident in Fig. 4 for the S-containing depolarizing additives with the wave peak approximately at −0.75 V for TU, −0.72 V for SPS, −0.71 V

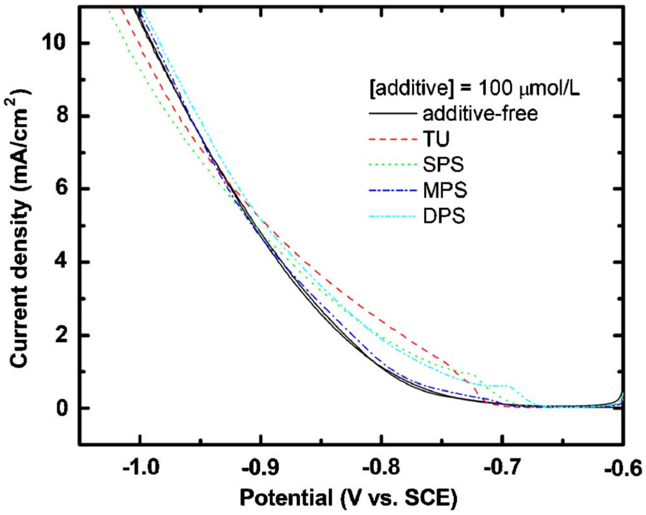

Figure 4. (Color online) Slow sweep voltammetry survey of the effect of sulfur-bearing additives on the rate of Ni deposition from 1 mol/L LNiSO$_4$·6H$_2$O + 0.2 mol/L NiCl$_2$·6H$_2$O + 0.5 mol/L H$_3$BO$_3$. The sweep rate was 1 mV/s.

for MPS, and −0.69 V for DPS. The magnitude of the depolarizing effects at −0.8 V increases in order of TU > SPS > DPS > MPS. As the overpotential increases the depolarizing effects of the additives diminish; TU and SPS actually begin to inhibit the nickel deposition rate at potentials below −0.92 V. A similar potential-dependent transition in TU behavior from acceleration to inhibition was also recently reported.[17]

Combination of inhibitors and accelerators.— Voltammetry was used to examine the interactions between the inhibiting cationic and nonionic surfactants, PEI, CTAC, and PEG, and the S-bearing accelerator species. The voltammetric behavior of Ni deposition in the presence of 5 μmol/L PEI with 100 μmol/L of the various depolarizing additives is shown in Fig. 5. The reduction wave near −0.7 V in the voltammetric response of the "accelerators-only" electrolyte (i.e., Fig. 4) is sharply suppressed in the presence of PEI. Nonetheless, the accelerators induce depassivation of the electrode at smaller overpotentials than that in the presence of PEI alone, as evident by the shift in the onset potential of abrupt depassivation toward more positive potentials. The strength of the depolarizing action increased in an order TU > DPS ≫ SPS > MPS. The most effective PEI depassivating agents, DPS and TU, have amine and dimethyl amine groups [-NH$_2$, -N(CH$_3$)$_2$], respectively, conjugated with the neighboring C═S bond in their molecular structures. No such functionality exists for the less effective depassivating additives SPS and MPS. It is possible that the lone pair electrons available in the amines for adsorption or protonation, similar to PEI, facilitate access and interaction of the S-bearing group of TU and DPS with the nickel surface beneath the PEI layer and thereby enable disruption of the PEI layer at smaller overpotentials. Similar behavior was observed for combinations of 100 μmol/L CTAC suppressor and 100 μmol/L accelerator as shown in Fig. 6; in this case, however, the order of depassivation activity was MPS/SPS > DPS > TU. Combinations of 100 μmol/L PEG and the 100 μmol/L S-bearing additives exhibited only a very slight acceleration at small overpotentials, as shown in Fig. 7. Surprisingly, all the systems, with the exception of TU-PEG, lead to slightly greater inhibition at more negative potentials then that provided by PEG alone.

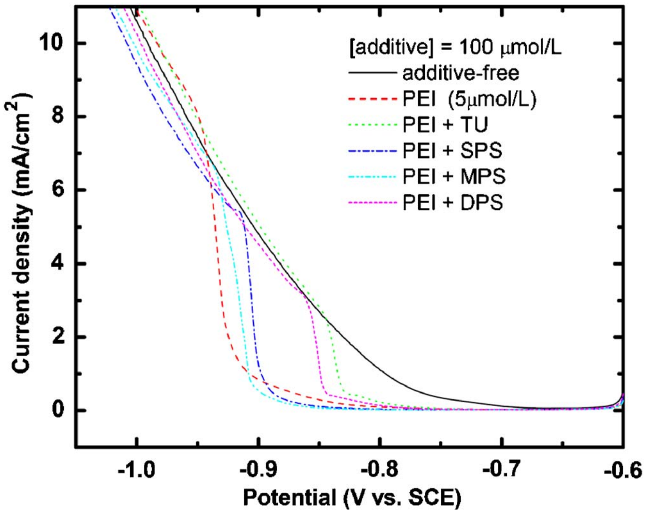

Figure 5. (Color online) Slow sweep voltammetry survey of the combined effect of PEI and depolarizing sulfur-bearing additives on the rate of Ni deposition. The electrolytes were composed of 1 mol/L NiSO$_4$·6H$_2$O + 0.2 mol/L NiCl$_2$·6H$_2$O + 0.5 mol/L H$_3$BO$_3$ and the sweep rate was 1 mV/s.

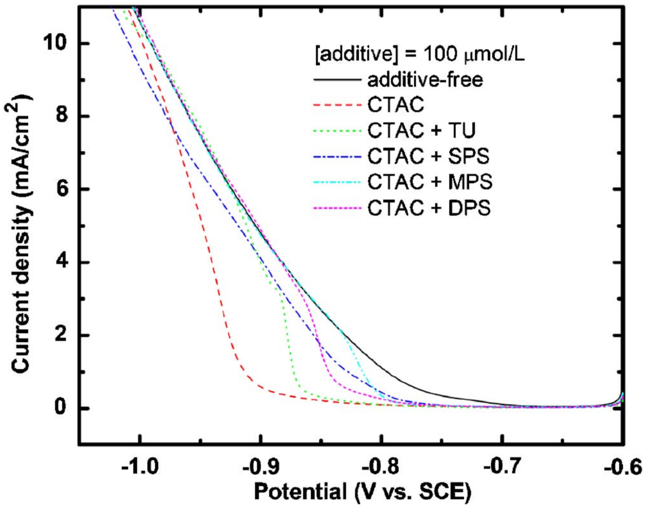

Figure 6. (Color online) Slow sweep voltammetry survey of the combined effect of CTAC and depolarizing sulfur-bearing additives on the rate of Ni deposition. The base electrolyte was 1 mol/L NiSO$_4$·6H$_2$O + 0.2 mol/L NiCl$_2$·6H$_2$O + 0.5 mol/L H$_3$BO$_3$ and the sweep rate was 1 mV/s.

Feature filling.— Based on the above survey, PEI, TU, and combinations thereof were chosen for further study of their effect on submicrometer feature filling. For the experiments shown here, Cu-seeded Damascene trench structures were examined; for consistency, the voltammetric results presented in the previous section were also obtained using copper substrates. The copper seed layers were used because the surface oxide can be easily reduced; the reduction of oxidized nickel substrates is more challenging, particularly for a pH greater than 2.5. A small number of Ni-seeded specimens was also examined to ascertain if any significant observations were associated with idiosyncrasies of nickel deposition on the copper seeds; none were.

Figure 8 shows a cross-sectional image of a Ni electrodeposit grown in additive-free solution for 3 min at −0.9 V. The Ni deposit on the 5 μm wide trench is conformal. The slightly smaller thickness on the sidewalls reflects the difference between the seed-layer thickness on the sidewalls vs the free surface and bottom due to line-of-sight constraints during physical vapor deposition (PVD) preparation. The growth front exhibits noticeable roughness. The

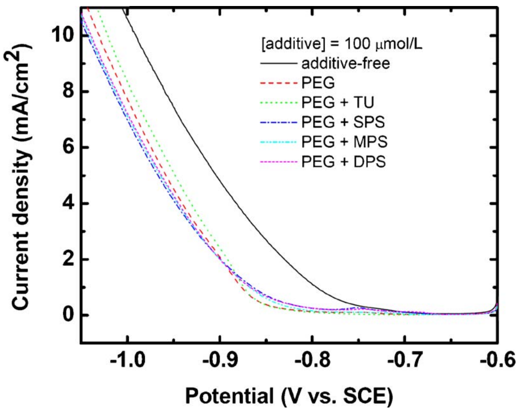

Figure 7. (Color online) Slow sweep voltammetry survey of the combined effect of PEG and depolarizing sulfur-bearing additives on the rate of Ni deposition. The base electrolyte was 1 mol/L $NiSO_4 \cdot 6H_2O$ + 0.2 mol/L $NiCl_2 \cdot 6H_2O$ + 0.5 mol/L H_3BO_3 and the sweep rate was 1 mV/s.

two widest, low-aspect-ratio trenches appear to be void-free while voids are evident (as marked) in the narrower high-aspect-ratio features. In light of the modest overpotential, negligible depletion of the Ni^{2+} accompanies the deposition, and thus the voids likely result from the roughness of the impinging sidewall surfaces.

Feature filling in the presence of PEI.— Additions of PEI induce significant changes in the feature-filling dynamics. Conformal filling of an ~1 μm wide trench in the additive-free electrolyte is shown in Fig. 9a. The addition of 5 μmol/L PEI yields superconformal film growth, as revealed in Fig. 9b, by preferential deposition at the bottom and on the deeper sections of the sidewall surfaces of the trench, while more limited deposition occurs on the neighboring free surface. Preferential deposition of nickel is also evident in the bottom corners of larger features such as that shown in Fig. 9c. Preliminary examination of finer features (not shown) suggests that void-free filling of the trenches persists up to an aspect ratio of at least 2.3 for a midheight trench width greater than 300 nm. The roughness of the growing sidewall surfaces most likely prevents void-free feature filling of the higher aspect ratio trenches. The shape change apparent in Fig. 9b might be explained as a variation of the diffusion-adsorption–consumption model for a single-component leveler.[40] However, further work detailing the feature-filling dynamics is required in order to establish this.

Similar experiments performed in 10 μmol/L PEI revealed further evidence of preferential deposition toward the bottoms of the finer features, as shown in Fig. 10a-d. The sloping deposits on the sidewalls suggest a PEI depletion effect in the higher aspect ratio features that is congruent with a consumption-driven leveler depletion mechanism, as suggested for Fig. 9b.[40] Negligible nickel deposition occurs on the top surface between the trenches shown in Fig. 10a-d; the convex bump there is almost entirely the copper seed layer. In the most favorable case (Fig. 10e), feature filling and planarity are obtained with modest overburden. However, significant dispersion in the feature-filling dynamics was observed, e.g., Fig. 10f, that might be partly related to inhomogeneities in the seed-layer/barrier of the wafer fragments.

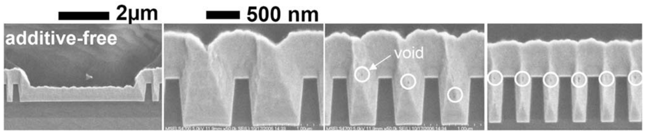

Figure 8. Trenches after 3 min Ni deposition at −0.9 V in additive-free electrolyte. Trench widths (left to right): 5 μm, 700 nm, 400 nm, and 230 nm. The white circles mark voids created when the opposing sidewall surfaces impinged (FESEM).

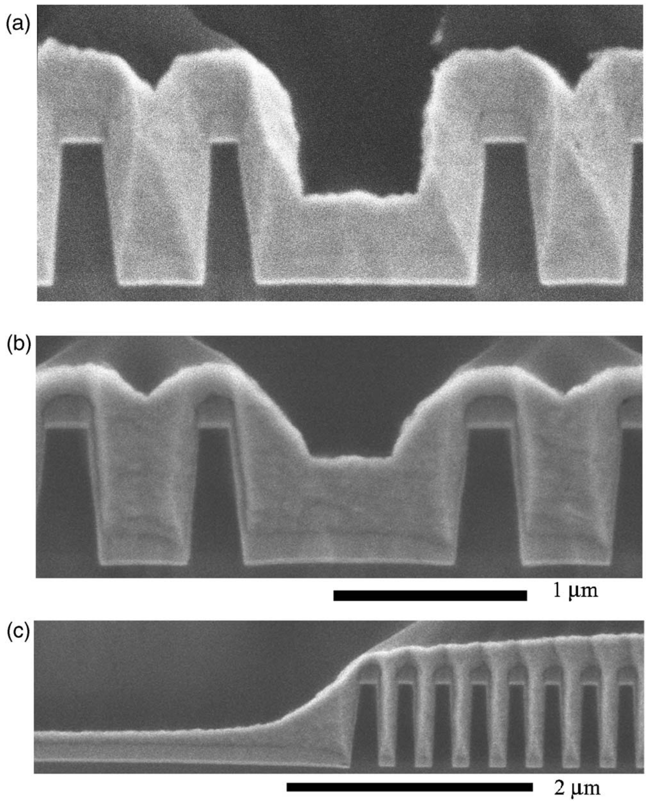

Figure 9. Trenches following 3 min of Ni deposition at −0.9 V: (a) conformal Ni deposition from an additive-free electrolyte, (b) superconformal Ni deposition in the presence of 5 μmol/L PEI, and (c) another region of the same specimen showing PEI-induced preferential deposition of Ni at the concave corner of wider features (FESEM).

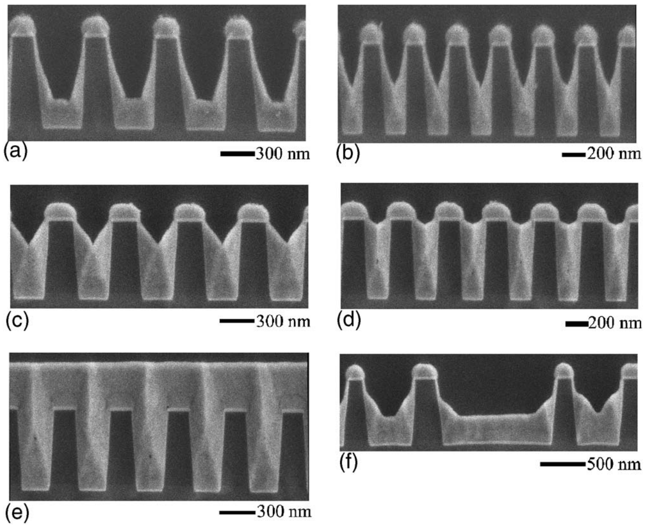

Figure 10. (a–d) PEI-induced superconformal growth can result in void-free feature filling. (e) Subsequent formation of a smooth planar surface. (f) An example of experimental dispersion where deposition only occurs in the lower half of the trenches. The Ni films were all deposited for 3 min at −0.9 V in electrolyte containing 10 μmol/L PEI (FESEM).

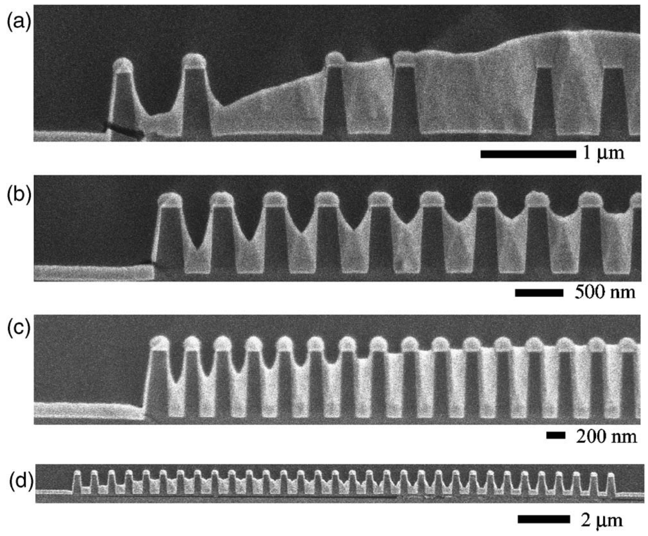

Figure 11. The convolution of trench filling with pattern density effects in an electrolyte containing 10 µmol/L PEI for Ni deposition at −0.9 V for 3 min. Feature filling appears to initiate in the centers of the densely patterned regions with the growth front moving vertically within the feature while the nucleation and growth process simultaneously propagates laterally between neighboring features. This unusual growth mode is associated with the NDR system behavior (FESEM).

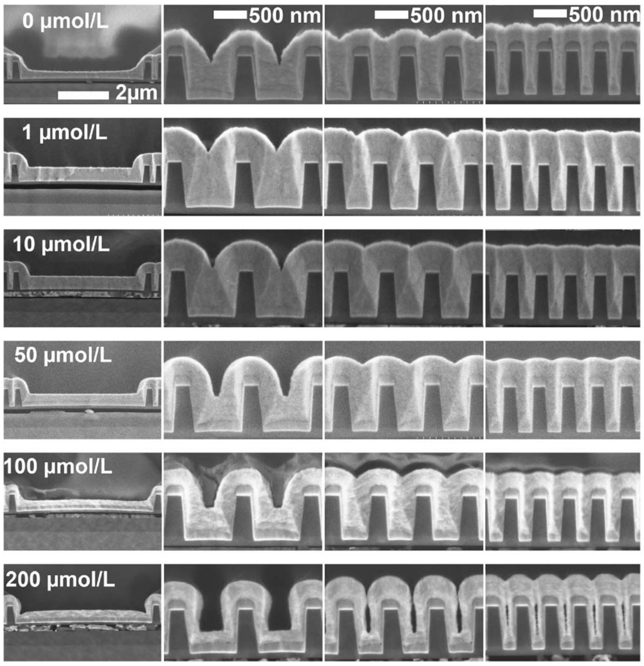

Figure 12. Trench filling in electrolytes containing 5 µmol/L PEI and µmol/L TU concentrations indicated. Ni deposition at −0.9 V for 3 min. Trench widths (left to right): 5 µm, 700 nm, 400 nm, and 230 nm (FESEM).

In addition to the superconformal feature-filling mode, deposition from 10 µmol/L PEI electrolyte revealed a variety of interesting pattern-density-dependent effects. For example, specimens grown at −0.9 V SCE for 3 min revealed multiple examples of preferential nucleation and bottom-up growth occurring in the finest and most densely packed trench arrays with negligible deposition evident on neighboring planar or lower feature density regions. Four examples of this behavior are shown in Fig. 11. The images reveal distinct active and passive areas evidently associated with the breakdown dynamics of the S-NDR voltammetric response outlined earlier; limited feature filling experimentation (not shown) reveals that the inhomogeneous deposition process diminishes as the applied potential is moved away from the S-NDR region identified in the iR-corrected slow sweep voltammetry. The same pattern density effects are observed when a nickel seed layer is used (not shown). The coupling of PEI depletion effects in feature filling with the potential distribution in the resistive electrolyte could provide a natural explanation for the inhomogeneous passive-active surface dynamics.[34-36] The inhomogeneity in growth, a manifestation of self-patterning, enables selective deposition triggered by the nonuniform substrate topography. The substrate pattern may be analogous to a perturbation analysis of the stability of the NDR system.[34-36] A more detailed description of this coupling behavior will be developed in a future publication.

Similar feature-filling results have been reported for Cu deposition using PEG and halide ions as cosuppressors.[41] The phenomenon was rationalized in terms of preferential halide consumption within the high-density patterned field; however, under the condition studied in Ref. 40, the PEG and halide system likely also exhibits S-NDR behavior. Therefore, coupling of halide depletion gradients and the corresponding potential distribution might also provide a more complete description of the unusual feature-filling process. Likewise, the fall-off in feature filling at the transition between two different feature sizes, like that shown in Fig. 11b and c, has also been reported for some high accelerator/suppressor ratio, low and medium acid (i.e., non-negligible solution resistance) Damascene copper plating baths.[42] Recent research on single-additive filling of through-vias in printed circuit boards has also revealed active-passive areas that are linked to the substrate topography.[43] The wide-ranging nature of these observation highlights the need for further study of this intriguing coupled gradient deposition mode, namely, leveler depletion effects combined with a topographically dependent potential distribution.

Feature filling with PEI and TU.— Trench filling was also examined for electrolytes with 5 µmol/L PEI and a range of TU concentration. Figure 12 summarizes the results for specimens deposited at −0.9 V for 3 min. The first row depicts trenches filled in the presence of the PEI alone. As noted in Fig. 9, the overall deposit thickness is reduced below that of the additive-free case (Fig. 8), particularly on the free surface, due to the inhibition of deposition by PEI. The surface roughness of the growth front is also reduced compared to the additive-free case, although a proper comparison must consider its dependence on film thickness. The PEI-induced superconformal deposition evident in the inhibited growth at the convex corners and more extensive deposition on the recessed surfaces was also noted earlier.

The addition of 1–50 µmol/L TU leads to two general morphological changes: (*i*) marked weakening of the superconformal growth mode and (*ii*) decreased local surface roughness. The addition of only 1 µmol/L TU causes film growth to shift back to the conformal mode. This is accompanied by smoothing of the local surface roughness that permits geometrical leveling to yield nominally void-free filling of trenches with sloping sidewalls; the finite surface roughness evident on the free surface suggests that closer microstructural analysis of the trench will reveal a seam that might include distributed nanometer-sized voids. Increasing the TU concentration to 10, 50, and 100 µmol/L leads to a further decrease in local roughness to the point that the surfaces all appear perfectly smooth, even at these high magnifications, and differentiation is not possible. For these additive concentrations filling approaches the analytical limit of geometric leveling whereby the sloping sidewalls enable "void-free" filling of trenches as narrow as 230 nm. Examination of narrower trenches (not shown in Fig. 12) revealed significant voiding along the centerline. This most likely arises from the combination of decreased lithographically defined sidewall angle and residual roughness from the heterogeneous nickel nucleation and growth on the aged copper seed layer. The condition for true

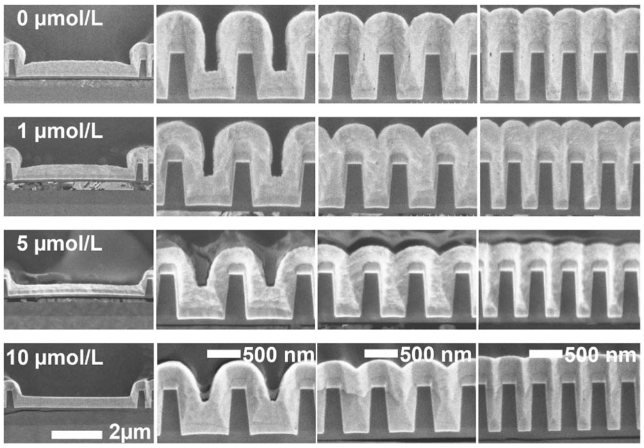

Figure 13. Trench filling in electrolytes containing 100 μmol/L TU and μmol/L PEI concentrations indicated. Nickel deposition at −0.9 V for 3 min. Trench widths (left to right): 5 μm, 700 nm, 400 nm, and 230 nm (FESEM).

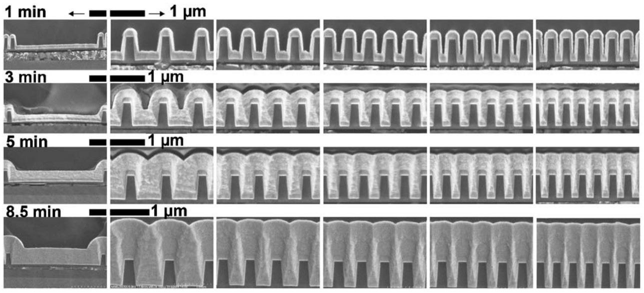

Figure 14. Filling of trenches in electrolyte containing 5 μmol/L PEI and 100 μmol/L TU as a function of deposition time at −0.90 V. Trench widths (left to right): 5 μm, 740 nm, 450 nm, 350 nm, 300 nm, and 250 nm (FESEM).

void-free filling by geometric leveling involves minimizing surface roughness and reactant depletion at the onset of sidewall impingement. An experimentally determined scaling relationship for film roughening/smoothing as a function of film thickness, TU concentration, etc., would permit analytical predictions of the feature size threshold for void-free trench filling as a function of sidewall angle.[44]

The images in Fig. 12 indicate that the growth rate passes through a maximum somewhere between 1 and 10 μmol/L TU. Higher TU concentrations result in a decreased overall deposition rate that is most conspicuous in the filling of the 700 nm wide trenches. TU concentrations of 200 μmol/L, and higher, result in a shift from conformal to subconformal growth. In this regime the coupling of the deposition-rate-suppressing characteristics of high TU concentration with the effect of area change during filling becomes dominant. Specifically, area reduction of advancing concave surfaces leads to enrichment of adsorbed TU with the associated suppression of the deposition reaction evident in the bottom trench corners. Conversely, the expanding surface area accompanying metal deposition at the convex upper corners dilutes the coverage of the adsorbed TU there, challenging the inhibition that it otherwise provides. Eventually, the more rapidly growing hemicylindrical fronts from the opposing upper corners impinge, leaving a large void in the trench. This type of additive-enhanced, subconformal growth was previously observed in the case of copper plating in the presence of PEG-Cl,[45] whereby much larger voids were created through the development of the convex protuberances for conditions where little depletion of the metal cations had occurred. The demonstration provided here (i.e., Fig. 12: 200 μmol/L TU) is perhaps even less ambiguous as there is truly negligible depletion of nickel cations at the free surface for these deposition conditions. The results reflect the nonmonotonic coverage or concentration-dependent effect of TU; namely, the deposition rate is accelerated at low concentrations but inhibited at higher concentrations. Thus, when the coverage of a saturated surface first decreases, the deposition rate passes through a maximum before decreasing monotonically toward the additive-free behavior.

The effect of PEI concentration on feature filling in the presence of 100 μmol/L TU was also examined; the results are summarized in Fig. 13. In the absence of PEI (0 μmol/L images) the thickness of Ni deposit on planar sections, such as the bottom of a 5 μm wide trench and the surrounding field, is nearly the same as that for the additive-free case (Fig. 8). This is congruent with the voltammetric results (Fig. 4), indicating TU has little effect on the current density on planar electrodes. However, deposition on nonplanar regions differs substantially; in concave regions, nickel deposition is inhibited relative to neighboring planar surfaces while on convex surfaces the metal deposition rate is accelerated. These effects combine to yield subconformal deposition, evident in the recessed notch in the bottom corners of wide trenches, and void formation along the centerlines of filled features. Consistent with these observations, it is here proposed that the 100 μmol/L TU single additive system has crossed from acceleration to suppression, a result that is consistent with the transition in Fig. 4 near the −0.9 V deposition potential, and that the TU-derived additive has a finite, i.e., nonzero, residence time on the surface, a requirement for area change to impact adsorbate coverage.

Adding 1 μmol/L PEI to the 100 μmol/L TU-containing electrolyte yields slightly inhibited deposition on planar surfaces as well as reduced acceleration on convex surfaces. The decreased size of the voids in the finer features is a direct result of these changes. PEI concentration of 5 μmol/L yields deposition that is further suppressed and more conformal. At PEI concentration of 5 and 10 μmol/L this effect is sustained, yielding smooth, conformal deposits. The smooth, conformal deposition coupled with the sloping sidewalls enables void-free filling.

Based on the results for the combined PEI-TU system, feature filling as a function of time and pattern dimension was investigated. As shown in Fig. 14, deposition at −0.9 V SCE in the presence of 5 μmol/L PEI and 100 μmol/L TU proceeds conformally, with geometric leveling beginning when the deposits on the sloped sidewalls meet. The growth velocity deduced for the 5 μm wide trench compares favorably with the 5 mA/cm^2 current density measured at −0.9 V in Fig. 5, confirming the high efficiency of the deposition process. The cross sections do not exhibit uniform voiding; however, the three finest arrays, with trench widths <350 nm, do contain small voids located randomly along the centerline, and heavily voided seams were evident in trenches less than 230 nm wide (not shown in Fig. 14).

Transmission electron microscopy (TEM) was used to further examine cross sections of the filled trenches. The specimens shown in Fig. 15 were prepared from patterned substrates after nickel deposition for 5 min at −0.9 V in the electrolyte containing 5 μmol/L PEI and 100 μmol/L M TU. Void-free filling is evident for the 650 nm deep, 300 nm wide trenches (average width determined from bottom width 250 nm, top width 350 nm, sidewall slope 3.5°) with aspect ratio (trench height /average width) ~2.2. The image of the 250 nm wide trenches (Fig. 15b) hints at seam formation along the midlines of several of the trenches; this could be a seam of low-density grain boundaries or discrete nanometer-size voids that do not span the full 100 + nm thickness of the TEM specimens. The ~150 nm wide trenches exhibit extensive void formation along their centerlines. In addition to the higher aspect ratio of this feature, it is also important to note the smaller sidewall slope of only 1.7° away from the vertical. The geometric factors, width, aspect ratio,

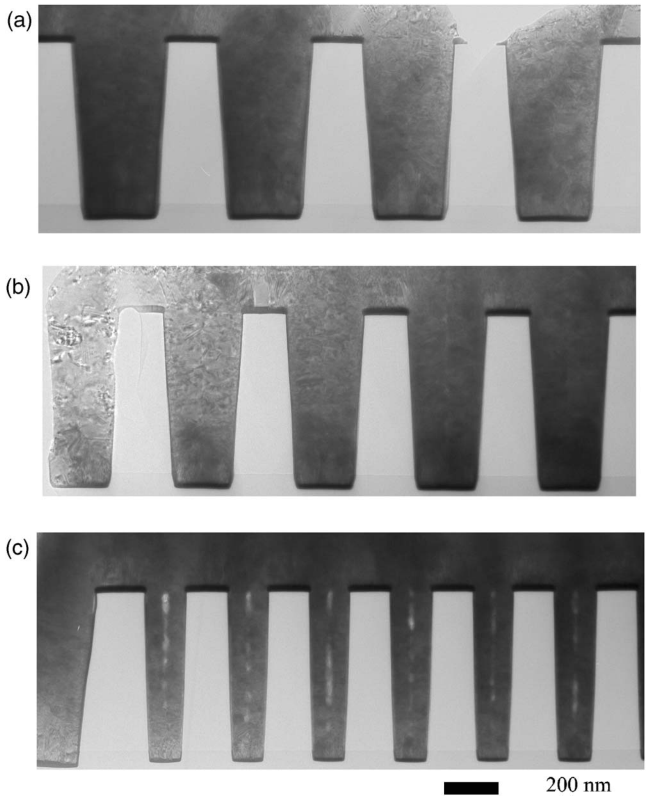

Figure 15. TEM cross sections of trenches filled by Ni deposition at −0.9 V for 5 min in an electrolyte containing 5 μmol/L PEI and 100 μmol/L TU. Trench widths and sidewall angles: (a) 250 nm, 3.5°; (b) 200 nm, 3.5°; and (c) 120 nm, 1.7°. The widest trenches are void-free while multiple voids are clearly evident along the centerline of the narrowest trenches. Some of the intermediate width trenches exhibit a low-density seam along their centerlines.

and sidewall angle, conspire with the finite surface roughness to generate a significant centerline defect density in these finest features.

According to the above results, geometrical leveling appears to be capable of yielding void-free filling of 650 nm deep, 300 nm wide trenches with sidewall angle of 3.5°. To explore the void-free filling threshold further, trenches of 300 and 350 nm width were sectioned and examined in a dual-beam focused ion beam (FIB)-SEM (Fig. 16); the imaging electron beam was inclined 52° from the substrate normal so trench heights are foreshortened. The irregular center top voids are discontinuous, appearing and disappearing with continued Ni removal (the lines beneath the voids are an artifact of the FIB milling process). The grooved trench profile on the top surface of a partially filled 500 nm wide trench in a similar FIB-SEM image (Fig. 17) reveals significant surface roughness that elucidates the origin of the void formation; the roughness and intermittent contact or coalescence along the groove demarcating the interface between the colliding sidewalls indicates how random voids arise through "pinch-off" connected with the impingement of the opposing sidewalls whose surface roughness is largely uncorrelated prior to contact.

Conclusions

The impact of a selection of prototypical cationic, anionic, and nonionic additives on the rate and morphological evolution of nickel electrodeposition was examined. Cationic species such as protonated, nitrogen-bearing PEI and CTA+ yield significant inhibition of nickel deposition. The inhibition is subject to abrupt breakdown, as revealed by the hysteretic voltammetric response. Correcting for ohmic electrolyte losses reveals an S-shaped NDR that correlates with a bifurcation reaction between an active and passive state.

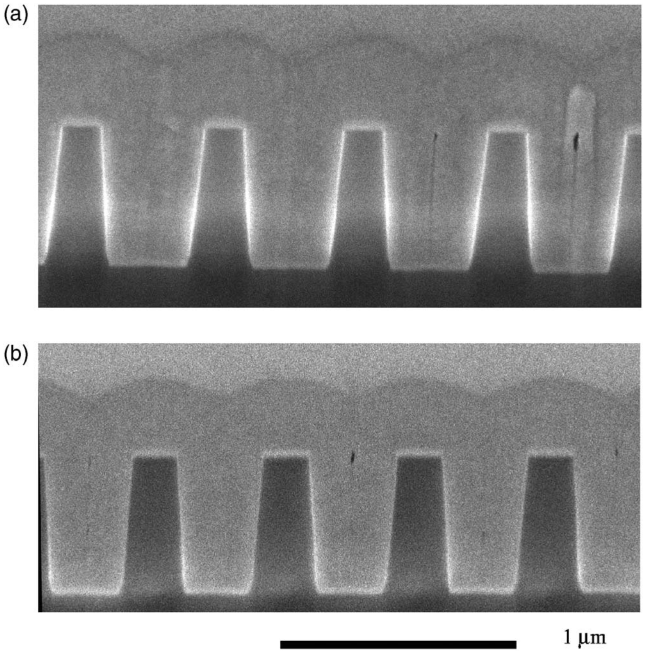

Figure 16. FIB-SEM images of trenches filled at −0.9 V for 3 min in an electrolyte containing 5 μmol/L PEI and 100 μmol/L TU. Sporadic voiding at the top of (a) 350 nm and (b) 300 nm wide trenches. The trenches appear foreshortened due to an abnormal imaging angle.

In contrast to the cationic surfactants, sulfur-bearing additives such as TU exert a depolarizing effect on nickel deposition, at least at low overpotentials and concentrations. When PEI and TU are both present the suppression and the associated voltammetric hysteresis provided by PEI is diminished, leading to uniform deposition on the wafer scale.

Two very different schemes for feature filling were identified. In the first instance a single additive electrolyte, based on cationic surfactant species such as PEI and CTAC, was shown to exhibit a nonlinear, potential-driven, S-shaped NDR bifurcation process between an active and passive state. For PEI this phenomenon was

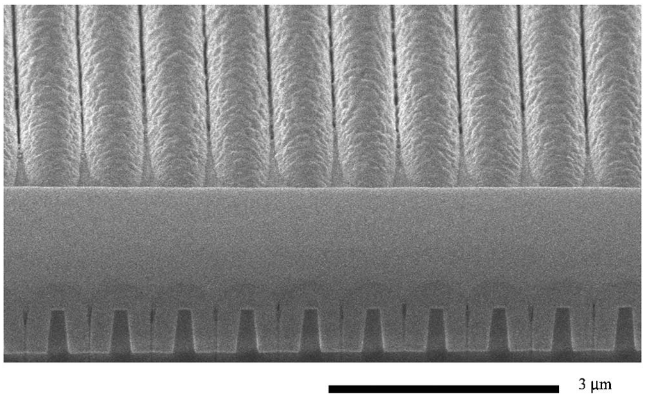

Figure 17. FIB-SEM image of a partially filled trench after deposition at −0.9 V for 3 min from an electrolyte containing 5 μmol/L PEI and 100 μmol/L TU. A thin layer of Pt was used to protect the surface of the Ga-milled cross section; the surface details of the grooved trenches are visible in the upper, uncoated half of the image. The grooved trench profile in the upper field reveals significant surface roughness that underlies the formation of random voids during sidewall impingement that accompanies feature filling.

shown to yield unusual bottom-up superconformal feature-filling behavior that also included pattern scale effects whereby feature filling began preferentially in the most densely patterned (high-surface-area) regions and was followed by lateral propagation of the metal nucleation and growth fronts. Many questions remain as to the detailed mechanism of feature filling that evidently derives from the close coupling of additive gradient and potential distribution.

Addition of TU to the PEI-containing electrolyte moved the system into a noncritical regime where feature filling occurred by homogenous, conformal deposition followed by geometrical leveling. Smoothing of the surface in the presence of TU played an important role in minimizing void formation during geometrical leveling. The likely extendability of these observations to the deposition of other iron group metals and alloys is a subject for future study.

Acknowledgments

The authors thank S. Claggett for assistance in preparation of specimens for FESEM.

The National Institute of Standards and Technology assisted in meeting the publication costs of this article.

References

1. L. T. Romankiw, *Electrochim. Acta*, **42**, 2985 (1997); J. O. Dukovic, *IBM J. Res. Dev.*, **37**, 125 (1993), and references therein.
2. P. C. Andricacos, C. Uzoh, J. O. Dukovic, J. Horkans, and H. Deligianni, *IBM J. Res. Dev.*, **42**, 567 (1998).
3. H. Masuda and K. Fukuda, *Science*, **268**, 1466 (1995).
4. T. P. Moffat, D. Wheeler, M. Edelstein, and D. Josell, *IBM J. Res. Dev.*, **49**, 19 (2005).
5. B. Baker, C. Witt, D. Wheeler, D. Josell, and T. P. Moffat, *Electrochem. Solid-State Lett.*, **6**, C67 (2003).
6. E. J. Ahn and J. J. Kim, *Electrochem. Solid-State Lett.*, **7**, C118 (2004).
7. D. Josell, D. Wheeler, and T. P. Moffat, *J. Electrochem. Soc.*, **153**, C11 (2006).
8. Z. M. Hu and T. Ritzdorf, *J. Electrochem. Soc.*, **153**, C467 (2006).
9. P. C. Andricacos and N. Robertson, *IBM J. Res. Dev.*, **42**, 671 (1998).
10. E. I. Cooper, C. Bonhote, J. Heidmann, Y. Hsu, P. Kern, J. W. Lam, M. Ramasubramanian, N. Robertson, L. T. Romankiw, and H. Xu, *IBM J. Res. Dev.*, **49**, 103 (2005).
11. S. A. Watson and J. Edwards, *Trans. Inst. Met. Finish.*, **34**, 167 (1957).
12. D. G. Foulke and O. Kardos, *Proc. Amer. Electroplaters' Soc.*, **43**, 172 (1956).
13. O. Kardos, *Proc. Amer. Electroplaters' Soc.*, **43**, 181 (1956).
14. J. Amblard, I. Epelboin, M. Froment, and G. Maurin, *J. Appl. Electrochem.*, **9**, 233 (1979).
15. I. Tabakovic, S. Riemer, V. Inturi, P. Jallen, and A. Thayer, *J. Electrochem. Soc.*, **147**, 219 (2000).
16. F. Lallemand, C. Comte, L. Ricq, P. Renaux, J. Pagetti, C. Dieppedale, and P. Gaud, *Appl. Surf. Sci.*, **225**, 59 (2004).
17. U. S. Mohanty, B. C. Tripathy, S. C. Das, and V. N. Misra, *Metall. Mater. Trans. B*, **36B**, 737 (2005).
18. U. S. Mohanty, B. C. Tripathy, P. Singh, and S. C. Das, *J. Appl. Electrochem.*, **31**, 969 (2001).
19. S. S. Kruglikov, N. T. Kudriavtsev, G. F. Vorobiova, and A. Ya. Antonov, *Electrochim. Acta*, **10**, 253 (1965).
20. J. Edwards, *Trans. Inst. Met. Finish.*, **41**, 169 (1964).
21. G. T. Rogers, M. J. Ware, and R. V. Fellows, *J. Electrochem. Soc.*, **107**, 677 (1960).
22. T. Osaka, T. Sawaguchi, F. Mizutani, T. Yokoshima, M. Takai, and Y. Okinaka, *J. Electrochem. Soc.*, **146**, 3295 (1999).
23. *Modern Electroplating*, M. Schlesinger and M. Paunovic, Editors, John Wiley & Sons, New York (2000).
24. P. L. Schilardi, O. Azzaroni, and R. C. Salvarezza, *Phys. Rev. B*, **62**, 13098 (2000).
25. Y. M. Loshkarov and E. M. Govorova, *Prot. Met.*, **34**, 399 (1998).
26. T. P. Moffat, D. Wheeler, and D. Josell, in *Superconformal Film Growth, Advances in Electrochemical Science and Engineering*, R. C. Alkire, D. Kolb, P. Ross, and J. Lipkowski, Editors, In press (2007), and references therein.
27. S. K. Cho, S.-K. Kim, and J. J. Kim, *J. Electrochem. Soc.*, **152**, C330 (2005).
28. S.-K. Kim, D. Josell, and T. P. Moffat, *J. Electrochem. Soc.*, **153**, C616 (2006).
29. S.-K. Kim, D. Josell, and T. P. Moffat, *J. Electrochem. Soc.*, **153**, C826 (2006).
30. N. Tantavichet and M. P. Pritzker, *Electrochim. Acta*, **50**, 1849 (2005).
31. S. Trasatti, *Electrified Interfaces in Physics, Chemistry, and Biology*, p. 945, R. Guidelli, Editor, NATO ASI Series, Kluwer Academic Publishers, Boston, MA (1992).
32. R. Meszaros, L. Thompson, M. Bos, and P. De Groot, *Langmuir*, **18**, 6164 (2002).
33. J. J. Kelly and A. C. West, *J. Electrochem. Soc.*, **145**, 3472 (1998).
34. K. Krischer, in *Advances in Electrochemical Science and Engineering*, R. C. Alkire and D. M. Kolb, Editors, Vol. 8, p. 142, Wiley-VCH Verlag GmbH & Co, Weinheim, Germany (2003).
35. D. Roha and U. Landau, *J. Electrochem. Soc.*, **137**, 824 (1990).
36. Y.-J. Li, J. Oslonovitch, N. Mazouz, F. Plenge, K. Krischer, and G. Ertl, *Science*, **291**, 2395 (2001).
37. A. T. Vagrayan and N. K. Baraboshkina, *Plating*, **1967**, 930 (August).
38. T. P. Moffat, D. Wheeler, C. Witt, and D. Josell, *Electrochem. Solid-State Lett.*, **5**, C110 (2002).
39. M. S. Kang, S.-K. Kim, and J. J. Kim, *Jpn. J. Appl. Phys., Part 1*, **44**, 8107 (2005).
40. R. Chalupa, Y. Cao, and A. C. West, *J. Appl. Electrochem.*, **32**, 135 (2002).
41. M. Hayase, M. Taketani, T. Hatsuzawa, and K. Hayabusa, *Electrochem. Solid-State Lett.*, **6**, C92 (2003).
42. C. Witt, J. Srinivasan, X. Lin, and R. Carpio, *ECS. Trans.* **2**(6), 107 (2007).
43. W.-P. Dow, H.-H. Chen, M.-Y. Yen, and C.-W. Liu, *ECS. Trans.* **2**(6), 259 (2007).
44. A. De Virgiliis, O. Azzaroni, R. C. Salvarezza, and E. V. Albano, *Appl. Phys. Lett.*, **82**, 1953 (2003).
45. T. P. Moffat, J. E. Bonevich, W. H. Huber, A. Stanishevsky, D. R. Kelly, G. R. Stafford, and D. Josell, *J. Electrochem. Soc.*, **147**, 4524 (2000).